


ORIGINAL ARTICLE OPEN ACCESS

A Front-Fixing Numerical Method for a Free-Boundary Nonlocal Diffusion Logistic Model

M.-C. Casabán¹ | R. Company¹ | V. Egorova²  | M. Fakharany^{3,4} | L. Jódar¹

¹Instituto Universitario de Matemática Multidisciplinar, Universitat Politècnica de València, Valencia, Spain | ²Departamento de Matemática Aplicada y Ciencias de la Computación, Universidad de Cantabria, Santander, Spain | ³Mathematics Department, Faculty of Science, Tanta University, Tanta, Egypt | ⁴Mathematics and Statistics Department, College of Science, Taibah University, Yanbu, Saudi Arabia

Correspondence: V. Egorova (vera.egorova@unican.es)

Received: 28 January 2025 | **Revised:** 21 July 2025 | **Accepted:** 24 July 2025

Funding: This research received no external funding.

Keywords: diffusive logistic model | finite difference method | Fisher-KPP model | front-fixing transformation | free boundary | Lax–Wendroff scheme | nonlocal diffusion

ABSTRACT

This paper introduces a numerical method, based on a front-fixing transformation together with a combination of the explicit finite difference schemes with the quadrature rules, to solve the Fisher-Kolmogorov, Petrovsky and Piskunov (KPP) population model that incorporates the combined complexities of nonlocal diffusion and free boundaries. The model utilizes nonlocal diffusion to capture intricate, potentially long-range, dispersal patterns of species. We propose two-stage front-fixing transformation that effectively maps the original integro-differential equation with two moving boundaries into a partial integro-differential equation on a fixed unit domain. The transformed system, which now includes an advection term and a spatially-scaled nonlocal integral, is then solved using a comparative analysis of several explicit finite difference schemes (explicit Euler scheme, upwind, and Lax–Wendroff) for the differential operator, coupled with Simpson’s rule for numerical integration. Additionally, this work contributes to understanding accelerated spreading rates, particularly for fat-tailed kernels, by numerically validating theoretical predictions and providing new insights into how kernel properties influence population dynamics. The proposed method demonstrates considerable flexibility and accuracy across various kernel types and growth scenarios, confirming its robustness and computational efficiency, which is an important prerequisite for future extensions to more complex problems.

1 | Introduction

The Fisher-KPP model [1, 2] is a well-established mathematical framework for studying population dynamics [3–8]. Traditionally, it assumes local diffusion, where the spread of individuals occurs only over short distances. However, real-world dispersal often involves occasional long-distance movements facilitated by mechanisms like wind, water currents, or animal vectors, which are not captured by local models. Nonlocal diffusion provides a more versatile framework to

This is an open access article under the terms of the [Creative Commons Attribution-NonCommercial-NoDerivs](https://creativecommons.org/licenses/by-nc-nd/4.0/) License, which permits use and distribution in any medium, provided the original work is properly cited, the use is non-commercial and no modifications or adaptations are made.

© 2025 The Author(s). *Studies in Applied Mathematics* published by Wiley Periodicals LLC.

incorporate these significant dispersal jumps, which can fundamentally alter population spread rates and spatial dynamics [9]. To address this, the Fisher-KPP equation has been extended to include nonlocal diffusion, allowing for more realistic population movement patterns [10–12].

An essential aspect of population dynamics that further complicates analysis is the presence of free boundaries, which represent the expanding or contracting edges of a habitat occupied by a species. For instance, this can model the expansion of an invasive species into new territory, or the contraction of a species' range due to climate change or habitat degradation [13, 14]. In the ecological context, the expansion of an invasive species into new territory can be modeled as a moving front along a river, coastline, or ecological corridor [15]. Conversely, the contraction of a species' range due to climate change or habitat degradation can also be captured through the retreat of these boundaries. Additionally, in the epidemiological context, the moving boundary represents the transition between infected and uninfected zones in simulating the spread of infectious diseases along migratory routes [16]. In the context of climate change, suitable habitats for many species are shifting in space and moving boundary models allow researchers to assess whether populations can track these changes or risk becoming trapped in suboptimal conditions [17]. These boundaries evolve based on population density and dispersal rates, introducing non-trivial conditions that require careful treatment to capture the interplay between diffusion and boundary movement. Similar complexities in modeling moving boundaries have been addressed in various fields, including polymer swelling [18], American option pricing [19, 20], drug dissolution and release [21], etc. Furthermore, recent advances in the study of Stefan-type problems with parabolic–logarithmic behavior illustrate the mathematical intricacies and practical relevance of handling such free-boundary conditions [22].

The interplay of nonlocal diffusion and boundary dynamics offers a versatile framework to model real-world population distributions more accurately, surpassing the constraints of local diffusion alone. In [23], a nonlocal diffusion model with free boundaries, building on the local diffusion framework of Du and Lin [24], was introduced. This model extends the Fisher-KPP equation to nonlocal diffusion with evolving boundaries, offering unique insights into population spread dynamics. Cao et al. [23] established a spreading–vanishing dichotomy, revealing distinct outcomes based on initial conditions and dispersal properties. Notably, the criteria for spreading versus vanishing in the nonlocal model deviate significantly from those in the local diffusion scenario outlined in [24].

Building on this, refs. [25, 26] conducted further studies on nonlocal diffusion models with free boundaries, emphasizing the spreading–vanishing dichotomy and focusing on the spread rate's dependence on the kernel function. They identified threshold conditions that result in either linear or accelerated spreading, providing a more nuanced understanding of population expansion under nonlocal effects. These works advance prior findings by defining explicit kernel function criteria that dictate whether spreading occurs at a finite or accelerated rate.

In this paper, we build upon the foundational studies by [23, 25, 26] by developing efficient numerical methods tailored for nonlocal diffusion models with free boundaries. To handle the challenges associated with moving boundaries, we introduce a front-fixing (FF) approach based on the Landau transform [27], which maps the domain with free boundaries onto a fixed domain. This method, recently applied to local diffusion models with free boundary [28], facilitates the use of well-established numerical techniques, enabling more efficient and accurate solutions.

FF methods have proven effective in addressing moving boundary problems in various contexts, including two-phase free boundary problems in finite domains [29], diffusion processes involving penetrants in rubber materials [30], migration phenomena with nonlinear boundary conditions [31], swelling solvent in a glassy polymer [22], American put options in financial mathematics [32, 33] and freeze-drying [34]. These approaches typically involve transforming the original problem into a fixed-domain formulation, simplifying the numerical implementation, and enhancing stability and accuracy. Once the domain is fixed, some numerical methods could be considered for spatial discretization [35, 36].

While various numerical techniques exist for aspects of our problem, they often address either free boundaries or nonlocal diffusion in isolation. For free-boundary PDE problems without nonlocal terms, traditional approaches apart from the described about FF transformation include front-tracking methods [28, 37], level set methods [38, 39], and particle-based methods like random walks [40]. Separately, for nonlocal diffusion problems, typically on fixed domains, recent numerical advancements include exponential time-differencing schemes [41], specialized finite element methods [42], and mesh-free optimization-based approaches [43]. However, the simultaneous presence of evolving free boundaries and a nonlocal integral operator poses a significant combined challenge, complicating the direct application or extension of many existing methods.

Inspired by these advancements in handling moving boundaries and nonlocal operators individually, this work specifically focuses on the challenge presented by their combination. We adapt the FF technique to the more complex framework of nonlocal diffusion with free boundaries. This particular adaptation, to our knowledge, has not been extensively explored or analyzed for this class of Fisher-KPP type models. Our primary aim is to develop and validate a numerical approach that effectively addresses both the evolving domain and the nonlocal interactions. To this end, after the FF transformation

maps the problem to a fixed domain, we employ explicit finite difference schemes for its solution. This choice was motivated by their relative implementation simplicity, which allows us to clearly investigate the stability and accuracy implications arising from the FF transformation itself, particularly concerning the newly introduced advection term within the nonlocal context. This advection term presents a challenge: it can lead to numerical instabilities if standard finite difference schemes, such as the forward-time centered-space (FTCS) scheme, are used. The FTCS scheme, although simple, is known to be conditionally unstable for advection-dominated problems because it cannot effectively handle the directional flow of information introduced by the advection term [36]. In particular, the central differencing in space fails to respect the direction of the advection term, leading to oscillations and instability as the solution propagates.

To overcome these stability issues, we employ upwind and Lax–Wendroff schemes, which are better suited for handling advection terms. The upwind scheme [44] is designed to respect the direction of information flow, thereby providing a more stable solution by effectively dampening oscillations in the presence of advection. This method, though slightly more diffusive, ensures that the solution remains stable and avoids spurious oscillations that can arise with central differencing. Alternatively, we also explore the Lax–Wendroff scheme [45], which is a second-order accurate method that offers a balance between stability and accuracy. This scheme achieves stability by combining the FTCS approach with a correction term that accounts for the second derivative of the advection term. This modification helps reduce numerical diffusion while maintaining stability.

The paper is organized as follows. In Section 2, we introduce the Fisher-KPP population model with nonlocal diffusion and free boundaries, along with the governing partial integro-differential equation (PIDE) and Stefan-like boundary conditions that describe the system. Section 3 outlines the FF transformation, where we detail the two-stage process for transforming the domain with free boundaries into a fixed domain. In Section 4, we present the numerical methods used to solve the transformed system. We describe the explicit finite difference schemes employed for the spatial and temporal discretization, as well as the Simpson's quadrature rule for approximating integrals. Section 5 contains numerical simulations and examples. Finally, Section 6 concludes the paper with a summary of the results and potential directions for future research.

2 | Fisher-KPP Population Model With Nonlocal Diffusion

The 1D Fisher-KPP population model with nonlocal diffusion and free boundaries studied in [23] presents a mathematical framework for understanding population dynamics where species spread in an environment with shifting boundaries. This model builds upon the classical Fisher-KPP equation, introducing nonlocal diffusion, which reflects more complex dispersal mechanisms seen in nature. The key equation governing this system is

$$\partial_t u = \alpha^2 \left(\int_{g(t)}^{h(t)} J(x-y) u(t, y) dy - u(t, x) \right) + f(u), \quad t > 0, \quad g(t) < x < h(t). \quad (1)$$

Here, $u(t, x)$ represents the population density at time t and location $x \in \mathbb{R}$, strictly positive parameter α^2 is the nonlocal diffusion coefficient, and the terms $g(t)$ and $h(t)$ define the moving boundaries of the population range. The function $J(x-y)$ represents the probability density that an individual at location y will move to location x . The kernel $J(x-y)$ is typically assumed to be symmetric, non-negative, and normalized such that:

$$\int_{\mathbb{R}} J(x) dx = 1.$$

Hence, the core of the nonlocal dispersal is described by the term $\alpha^2 \left(\int_{g(t)}^{h(t)} J(x-y) u(t, y) dy - u(t, x) \right)$, where the integral represents the rate at which individuals arrive at location x from all other locations y within the current habitat $[g(t), h(t)]$. The term $-u(t, x)$ describes the rate at which individuals are leaving location x to travel to other sites [9]. Thus, the operator $\left(\int_{g(t)}^{h(t)} J(x-y) u(t, y) dy - u(t, x) \right)$ can be viewed as the nonlocal counterpart to the standard Laplacian diffusion operator u_{xx} , modeling how individuals in a population disperse over space through potentially long-range jumps. This approach contrasts with classical local diffusion models, where dispersal is limited to immediately neighboring areas.

The growth function $f(u)$ dictates the local reproduction rate of the population, usually of the logistic type

$$f(u) = ru(1 - u/K), \quad (2)$$

where r is the growth rate, and K is the carrying capacity. The growth function $f(u)$ is positive for $u \in (0, K)$ and has to fulfill the following conditions [23, 25]: $f(u)$ is independent of (t, x) , $f(u)/u$ is strictly decreasing for $u \in \mathbb{R}^+$, moreover,

$$f(0) = f(K) = 0; \quad f'(u) \text{ exists, and } f'(0) > 0. \quad (3)$$

The system is further governed by boundary conditions

$$u(t, g(t)) = u(t, h(t)) = 0, \quad (4)$$

indicating that the population density at the boundaries is zero, and initial conditions

$$u(0, x) = u_0(x), \quad g(0) = -h_0, \quad h(0) = h_0, \quad h_0 > 0; \quad (5)$$

specifying the initial distribution of the population and the positions of the boundaries at the moment $t = 0$.

The dynamics of the boundaries are described by Stefan-like conditions, which depend on the outward flux of the population at the boundaries:

$$\frac{dh}{dt} = \mu \int_{g(t)}^{h(t)} \int_{h(t)}^{+\infty} J(x-y)u(t, x)dydx, \quad (6)$$

$$\frac{dg}{dt} = -\mu \int_{g(t)}^{h(t)} \int_{-\infty}^{g(t)} J(x-y)u(t, x)dydx. \quad (7)$$

Based on the nature of the integrand function $J(x-y)u(t, x)$ in Equations (6) and (7), we observe that these functions are independent, consequently, we can write them in the following manner:

$$\frac{dh}{dt} = \mu \int_{g(t)}^{h(t)} u(t, x) \left(\int_{h(t)}^{+\infty} J(x-y)dy \right) dx, \quad (8)$$

$$\frac{dg}{dt} = -\mu \int_{g(t)}^{h(t)} u(t, x) \left(\int_{-\infty}^{g(t)} J(x-y)dy \right) dx. \quad (9)$$

These conditions state that the speed at which the habitat boundaries, $g(t)$ and $h(t)$, move is proportional to the flux of individuals successfully dispersing across them. The constant μ represents this proportionality factor. Biologically, individuals at a location x within the habitat $[g(t), h(t)]$ can disperse. The kernel $J(x-y)$ describes the probability distribution for an individual moving from x to y . Consequently, the inner integral in the boundary conditions represents the probability that an individual currently at x will disperse beyond the existing habitat edge.

As established in [9, 23], not all individuals that disperse into new areas will successfully establish themselves and contribute to range expansion. Various environmental factors, for instance, resource availability in the newly entered territory, can limit establishment success. For modeling simplicity, we assume that parameter μ , which encapsulates both this establishment success rate and the general sensitivity of the boundary to the outward dispersal pressure from the population, is constant for a given species. Thus, the overall rate of the boundary movement is modeled as proportional to the total number of individuals effectively expanding the range.

In [23, 25, 26], the long-term behavior of the solution is analyzed through the framework of the spreading-vanishing dichotomy, yielding several significant results. To contextualize these findings, we recall some key definitions and theorems.

Theorem 1.2 in [23] asserts that under certain conditions on the initial population range and related parameters, the population undergoes spreading, meaning:

$$\lim_{t \rightarrow \infty} (g(t), h(t)) = \mathbb{R}, \quad \text{and} \quad u(t, x) \rightarrow v_0 \text{ locally uniformly,}$$

where v_0 is the positive steady state of the growth function $f(u)$.

Conversely, if the initial population range or other parameters fail to meet these conditions, the population undergoes vanishing, with the range remaining bounded. Specifically:

$$\lim_{t \rightarrow \infty} (g(t), h(t)) = (g_\infty, h_\infty), \quad \text{with} \quad u(t, x) \rightarrow 0 \text{ uniformly for } x \in [g(t), h(t)].$$

The criteria for determining whether spreading or vanishing occurs are influenced by the initial population range h_0 , the growth rate $f'(0)$ at zero population density, and the amount of the rate μ . These factors interact as follows [23, Theorem 1.3]:

- If $f'(0) \geq \alpha^2$, spreading always occurs regardless of other parameters.
- If $f'(0) \in (0, \alpha^2)$, there exists a critical value $h^* > 0$ such that:
 - Spreading occurs if the initial range is large enough, i.e., if $h_0 \geq h^*/2$.
 - For $h_0 < h^*/2$, spreading happens only if μ exceeds a critical value μ^* .

The kernel $J(x - y)$ models the movement of the population from one point to another, and its shape and properties affect the long-term behavior of the population. If the kernel is localized (i.e., it decays quickly for large distances or has compact support), the spreading will be slower, as individuals will only influence nearby locations.

The interaction between the growth function $f(u)$ and the kernel $J(x - y)$ affects the long-term dynamics. The growth function dictates the reproduction and death rates of the population, while the kernel determines how fast the population can spread across space. If the kernel J allows for fast dispersal, the spreading may occur even for small initial population ranges, leading to spreading as long as the growth rate $f'(0)$ is favorable.

In [25], the authors established that if the kernel function satisfies

$$\int_0^\infty xJ(x)dx < \infty, \quad (10)$$

then, in the case of spreading, the spreading speed is asymptotically constant and determines the linear rate:

$$\lim_{t \rightarrow \infty} \frac{h(t)}{t} = - \lim_{t \rightarrow \infty} \frac{g(t)}{t} = c_0, \quad (11)$$

where $c_0 > 0$ is uniquely determined by the kernel and growth parameters. Otherwise, if condition (10) is not fulfilled, the spreading becomes accelerated, meaning the population expands faster than linearly.

Recent works by Du and Ni [26, 46] examine the phenomenon of accelerated spreading. For a free boundary problem described by moving boundaries $g(t)$ and $h(t)$, accelerated spreading implies:

$$\lim_{t \rightarrow \infty} \frac{h(t)}{t} = \lim_{t \rightarrow \infty} \frac{-g(t)}{t} = \infty.$$

Accelerated spreading occurs when the kernel $J(x)$ does not satisfy the finite first-moment condition (10). Additionally, the thin-tail condition

$$\exists \phi > 0 \text{ such that } \int_{-\infty}^\infty J(x)e^{\phi x}dx < \infty, \quad (12)$$

is related to the existence of traveling waves, see for details [26, p. 2937]. When (12) is violated, accelerated spreading becomes more likely. If the kernel satisfies (10) but not the stricter “thin-tail” condition (12), the spreading remains linear but may still differ qualitatively from the local Fisher-KPP spreading, see [47].

Specific rates of acceleration depend on the asymptotic behavior of the kernel [26, 46]. For kernel functions $J(x)$ with heavy tails, accelerated spreading occurs at rates determined by the tail behavior of $J(x)$. In particular, we can consider the following scenarios [26]: if $J(x) \sim |x|^{-\gamma}$ as $|x| \rightarrow \infty$ with $\gamma \in (1, 2)$, the spreading rates are:

$$\lim_{t \rightarrow \infty} \frac{h(t)}{t^{1/(\gamma-1)}} = \lim_{t \rightarrow \infty} \frac{-g(t)}{t^{1/(\gamma-1)}} = \frac{2^{2-\gamma}}{2-\gamma} \mu \lambda, \quad (13)$$

where $\lambda > 0$ is a parameter related to the kernel.

For $\gamma = 2$, one gets

$$\lim_{t \rightarrow \infty} \frac{h(t)}{t \ln t} = \lim_{t \rightarrow \infty} \frac{-g(t)}{t \ln t} = \mu \lambda. \quad (14)$$

The well-posedness, including existence and uniqueness of solutions to this nonlocal free boundary problem, along with the spreading–vanishing dichotomy, has been established in foundational works such as [23, 25, 26]. In particular, see Theorem 1.1 in [23]. This paper focuses on developing and analyzing numerical methods for its solution. Further, we present a numerical algorithm for solving the problem and conduct several simulations to investigate the spreading–vanishing dichotomy, focusing on its dependence on the kernel properties, the growth function, and the initial habitat size.

3 | Front-Fixing Transformation

To address the complexities of dealing with two moving boundaries, an FF transformation is employed. This technique transforms the domain with free boundaries into a fixed domain, facilitating the use of numerical methods. The transformation is performed in two stages: first, introducing new variables to fix one boundary, and second, applying additional transformations to ensure the entire domain is of unit length independent of the time. This approach allows for the effective application of numerical methods to solve the system and analyze the population dynamics.

3.1 | First Stage

In the first stage of the method, we introduce a new variable and function to simplify the moving boundaries. The new variable is defined as $z = x - g(t)$, which shifts the left boundary to $z = 0$. We also define a new function $v(t, z) = u(t, x)$, where $u(t, x)$ is the original population density. This transformation changes the domain $g(t) \leq x \leq h(t)$ into an interval with the fixed left boundary $0 \leq z \leq l(t)$, where $l(t) = h(t) - g(t)$ represents the length of the interval.

The partial derivatives of u are transformed as follows:

$$\frac{\partial u}{\partial x} = \frac{\partial v}{\partial z}, \quad \frac{\partial u}{\partial t} = \frac{\partial v}{\partial t} - g'(t) \frac{\partial v}{\partial z}. \quad (15)$$

Next, the integral term in the original equation becomes

$$\int_{g(t)}^{h(t)} J(x - y)u(t, y) dy = \int_0^{l(t)} J(z - \eta)v(t, \eta) d\eta. \quad (16)$$

Now, by combining these changes, the original integro-differential Equation (1) is transformed into the following PIDE for the new unknown $v(t, z)$:

$$\frac{\partial v}{\partial t} - g'(t) \frac{\partial v}{\partial z} = \alpha^2 \left(\int_0^{l(t)} J(z - \eta)v(t, \eta) d\eta - v(t, z) \right) + f(v), \quad 0 \leq z \leq l(t). \quad (17)$$

The free boundary conditions (8)–(9) are also transformed. The equation for $g'(t)$, the speed of the left boundary, becomes

$$g'(t) = -\mu \int_0^{l(t)} v(t, z) \int_{-\infty}^0 J(z - \eta) d\eta dz. \quad (18)$$

Here, $g'(t)$ describes the evolution of the moving boundary $g(t)$ over time. For the right boundary, $h'(t) = g'(t) + l'(t)$, and the length $l(t)$ of the original interval varies with the time as follows:

$$l'(t) = \mu \int_0^{l(t)} v(t, z) \int_{l(t)}^{+\infty} J(z - \eta) d\eta dz + \mu \int_0^{l(t)} v(t, z) \int_{-\infty}^0 J(z - \eta) d\eta dz. \quad (19)$$

Taking into account that $\int_{\mathbb{R}} J(x) dx = 1$, we simplify the expression for $l'(t)$

$$l'(t) = \mu \int_0^{l(t)} v(t, z) \left(\int_{l(t)}^{+\infty} J(z - \eta) d\eta + \int_{-\infty}^0 J(z - \eta) d\eta \right) dz = \mu \int_0^{l(t)} v(t, z) \left(1 - \int_0^{l(t)} J(z - \eta) d\eta \right) dz. \quad (20)$$

3.2 | Second Stage

To establish a fixed domain, we apply the Landau transformation [27] introducing a new variable $r = \frac{z}{l(t)}$, $0 \leq r \leq 1$, and the function $w(t, r) = v(t, z)$. The partial derivatives of v with respect to t and z are expressed in terms of w :

$$\frac{\partial v}{\partial z} = \frac{1}{l(t)} \frac{\partial w}{\partial r}, \quad \frac{\partial v}{\partial t} = \frac{\partial w}{\partial t} - r \frac{l'(t)}{l(t)} \frac{\partial w}{\partial r}.$$

The integral in (17) is transformed to the following:

$$\int_0^{l(t)} J(z - \eta) v(t, \eta) d\eta = l(t) \int_0^1 J(l(t)(r - \rho)) w(t, \rho) d\rho. \quad (21)$$

Hence, the transformed equation in the fixed domain is written as follows:

$$\frac{\partial w}{\partial t} - \left(r \frac{l'(t)}{l(t)} + \frac{g'(t)}{l(t)} \right) \frac{\partial w}{\partial r} = \alpha^2 \left[l(t) \int_0^1 J(l(t)(r - \rho)) w(t, \rho) d\rho - w(t, r) \right] + f(w), \quad t > 0, 0 \leq r \leq 1. \quad (22)$$

Stefan conditions (18) and (19) are transformed as follows:

$$g'(t) = -\mu l^2(t) \int_0^1 w(t, \rho) \int_\rho^\infty J(l(t)\eta) d\eta d\rho, \quad l'(t) = \mu l(t) \int_0^1 w(t, \rho) \left(1 - l(t) \int_{\rho-1}^\rho J(l(t)\eta) d\eta \right) d\rho. \quad (23)$$

Let us define the CDF $K[x]$ of the kernel function $J(s)$ as follows:

$$K[x] = \int_{-\infty}^x J(s) ds, \quad (24)$$

where $J(s)$ is assumed to be a symmetric probability density function over \mathbb{R} , with the following properties:

- For any $a, b \in \mathbb{R}$, the integral of $J(s)$ over $[a, b]$ can be expressed in terms of K as

$$\int_a^b J(s) ds = K[b] - K[a].$$

- For any scalar $\lambda > 0$, the integral of a scaled version of $J(s)$ over $[a, b]$ is given by

$$\int_a^b J(\lambda s) ds = \frac{1}{\lambda} (K[\lambda b] - K[\lambda a]).$$

- Due to the symmetry of $J(s)$ around zero (i.e., $J(s) = J(-s)$), we have

$$K[0] = \frac{1}{2}.$$

This symmetry implies that the cumulative probability up to zero is half of the total mass, consistent with $J(s)$ being a symmetric probability distribution.

The Stefan conditions from (23) can be expressed in the transformed coordinates as follows:

$$g'(t) = -\mu l(t) \int_0^1 w(t, \rho) (1 - K[l(t)\rho]) d\rho, \quad (25)$$

$$l'(t) = \mu l(t) \int_0^1 w(t, \rho) (1 - K[l(t)\rho] + K[l(t)(\rho - 1)]) d\rho. \quad (26)$$

Next, we substitute the expressions for $g'(t)$ and $l'(t)$ from (25) and (26) into the transformed PIDE, given in (22), resulting in the following form:

$$\begin{aligned} \frac{\partial w}{\partial t} = & \mu \left[r \int_0^1 w(t, \rho)(1 - K[l(t)\rho] + K[l(t)(\rho - 1)]) d\rho - \int_0^1 w(t, \rho)(1 - K[l(t)\rho]) d\rho \right] \frac{\partial w}{\partial r} \\ & + \alpha^2 \left[l(t) \int_0^1 J(l(t)(r - \rho))w(t, \rho) d\rho - w(t, r) \right] + f(w), \quad t > 0, 0 \leq r \leq 1. \end{aligned} \quad (27)$$

The term involving the advection effect, controlled by the integrals of $w(t, \rho)$ and the cumulative kernel K , captures the impact of boundary movement in the transformed coordinates.

The initial and boundary conditions from (4)–(5) are now rewritten as follows:

$$w(t, 0) = w(t, 1) = 0, \quad w(0, r) = u_0((h_0 - g_0)r + g_0), \quad l(0) = l_0 = h_0 - g_0. \quad (28)$$

4 | Numerical Algorithm

The transformed PIDE problem (27) with conditions given in (25)–(26) and (28) is solved numerically by using a finite difference method (FDM).

Let t range from 0 to T with a time step $\Delta t = \frac{T}{N}$. Similarly, r ranges from 0 to 1 with a space step $\Delta r = \frac{1}{M}$. Here, T is the final simulation time, N is the total number of time steps, and M is the number of spatial subintervals in the transformed domain $[0, 1]$.

We define a uniform grid

$$r_i = i\Delta r, \quad i = 0, 1, 2, \dots, M, \quad t^n = n\Delta t, \quad n = 0, 1, 2, \dots, N. \quad (29)$$

The approximated numerical solution at each grid node is denoted by $w_i^n \approx w(t_n, r_i)$ and the distance between two free boundaries $g^n \approx g(t^n)$ and $h^n \approx h(t^n)$ is denoted by $l^n \approx l(t^n)$.

The integrals can be approximated numerically using various quadrature rules, such as the midpoint rule or the trapezoidal rule. In this case, we choose Simpson's rule for its improved accuracy compared to other methods. While the midpoint and trapezoidal rules exhibit second-order convergence for the approximation error, Simpson's rule provides fourth-order convergence, leading to more accurate integral approximations for a given number of sub-intervals, see [48, Chapter 2]. Let us introduce the following notation:

$$S(w^n) = \frac{\Delta r}{3} \left(w_0^n + 4 \sum_{\text{odd } i} w_i^n + 2 \sum_{\text{even } i} w_i^n + w_M^n \right), \quad (30)$$

where $w^n = [w_0^n, w_1^n, \dots, w_M^n]$. Then, Stefan conditions (25)–(26) are discretized as follows:

$$\frac{g^{n+1} - g^n}{\Delta t} = -\mu l^n S(p^n), \quad \frac{l^{n+1} - l^n}{\Delta t} = \mu l^n S(q^n), \quad (31)$$

where p^n and q^n are two vectors of the components

$$p_j^n = w_j^n(1 - K[l^n r_j]), \quad q_j^n = w_j^n(1 - K[l^n r_j] + K[l^n(r_j - 1)]), \quad j = 0, \dots, M. \quad (32)$$

Hence, the advection coefficient is approximated at the node (r_i, t^n) by using the Simpson's rule

$$\mu \left[r_i \int_0^1 w(t^n, \rho)(1 - K[l(t^n)\rho] + K[l(t^n)(\rho - 1)]) d\rho - \int_0^1 w(t^n, \rho)(1 - K[l(t^n)\rho]) d\rho \right] \approx \mu(r_i S(q^n) - S(p^n)) = A^n(r_i). \quad (33)$$

Initial and boundary conditions (28) for all considered methods are given by

$$w_0^n = w_M^n = 0, \quad n = 0, 1, 2, \dots, N; \quad w_i^0 = u_0((h_0 - g_0)r_i + g_0), \quad i = 0, 1, 2, \dots, M; \quad l^0 = h_0 - g_0. \quad (34)$$

4.1 | Forward-Time Centered-Space Scheme

The simplest algorithm for the discretization of the differential operator of Equation (27) is the FTCS scheme. It uses the forward difference for the time step:

$$\frac{\partial w}{\partial t} \approx \frac{w_i^{n+1} - w_i^n}{\Delta t}. \quad (35)$$

For the advection term $\frac{\partial w}{\partial r}$, the centered difference scheme is applied:

$$\frac{\partial w}{\partial r} \approx \frac{w_{i+1}^n - w_{i-1}^n}{2\Delta r}. \quad (36)$$

Substituting these into the transformed PIDE (27) gives the FTCS scheme:

$$\frac{w_i^{n+1} - w_i^n}{\Delta t} = A^n(r_i) \frac{w_{i+1}^n - w_{i-1}^n}{2\Delta r} + \alpha^2 [l^n S(y^n(r_i)) - w_i^n] + f(w_i^n), \quad (37)$$

where $y^n(r_i)$ is the vector of the components $y_j^n(r_i) = w_j^n J(l^n(r_i - r_j))$, $j = 0, \dots, M$.

Let us introduce the Courant number $C_i^n = A^n(r_i) \frac{\Delta t}{\Delta r}$, see for details [36, 44], then the scheme (37) is written as follows:

$$w_i^{n+1} = w_i^n + \frac{C_i^n}{2} (w_{i+1}^n - w_{i-1}^n) + \Delta t \alpha^2 [l^n S(y^n(r_i)) - w_i^n] + \Delta t f(w_i^n). \quad (38)$$

The FTCS scheme, while explicit and straightforward to implement, suffers from significant stability limitations, particularly in advection-dominated problems. As noted in [36, p. 280], the FTCS scheme is unconditionally unstable for pure convection problems. This contrasts with its conditional stability for the diffusion equation. Due to its inherent instability, the FTCS scheme is generally impractical for problems of the form (27).

4.2 | Upwind Differencing Scheme

In order to avoid the stability issues, we employ the upwind scheme [36, p. 280] to the differential operator in (27). The key idea is to account for the direction of the flow when determining which values to use for numerical computations. When the advection coefficient $A^n(r_i)$ is positive, the scheme takes information from the point ahead. Conversely, when the advection coefficient is negative, values are taken from the point behind. This helps to stabilize the numerical solution and prevent non-physical oscillations by ensuring that information propagates correctly in the direction of the flow.

The PIDE (27) is then discretized as follows:

$$\frac{w_i^{n+1} - w_i^n}{\Delta t} = \begin{cases} A^n(r_i) \frac{w_{i+1}^n - w_i^n}{\Delta r} + \alpha^2 [l^n S(y^n(r_i)) - w_i^n] + f(w_i^n), & \text{if } A^n(r_i) > 0, \\ A^n(r_i) \frac{w_i^n - w_{i-1}^n}{\Delta r} + \alpha^2 [l^n S(y^n(r_i)) - w_i^n] + f(w_i^n), & \text{if } A^n(r_i) \leq 0. \end{cases} \quad (39)$$

The upwind scheme can be written in the following form:

$$w_i^{n+1} = w_i^n (1 - |C_i^n|) + |C_i^n| w_{i+\text{sign}(A^n(r_i))}^n + \Delta t \alpha^2 [l^n S(y^n(r_i)) - w_i^n] + \Delta t f(w_i^n), \quad (40)$$

where $\text{sign}(A^n(r_i)) = \begin{cases} +1, & \text{if } A^n(r_i) > 0, \\ -1, & \text{if } A^n(r_i) < 0. \end{cases}$

4.2.1 | Positivity

To establish bounds for p_j^n and q_j^n , we leverage the properties of $K[x]$, the cumulative distribution function (CDF) of the symmetric kernel J . As a CDF, $K[x]$ is non-decreasing and its range is $[0,1]$. Due to the symmetry of J , $K[0] = 1/2$. Since $l^n > 0$ and $r_j \geq 0$ within the computational domain ($j = 0, \dots, M$), it follows that $l^n r_j \geq 0$, which implies $K[l^n r_j] \geq K[0] = 1/2$. Assuming the population density w_j^n is non-negative and does not exceed a normalized carrying capacity (thus $0 \leq w_j^n \leq 1$), then:

$$0 \leq p_j^n \leq 1 - K[l^n r_j] \leq 1 - K[0] = \frac{1}{2}, \quad (41)$$

$$0 \leq q_j^n \leq 1 - K[l^n r_j] + K[l^n(r_j - 1)] \leq 1. \quad (42)$$

Since $S(w^n)$ is the Simpson's rule for the integration over the interval $[0, 1]$, then the following estimations take place:

$$0 \leq S(p^n) \leq S\left(\frac{1}{2}\right) = \frac{\Delta r}{3} \cdot \frac{1}{2} \left(1 + 4 \sum_{\text{odd } i} 1 + 2 \sum_{\text{even } i} 1 + 1 \right) = \frac{1}{2}, \quad (43)$$

$$0 \leq S(q^n) \leq S(1) = 1. \quad (44)$$

Hence, if $A^n(r_i) > 0$, one gets

$$|A^n(r_i)| = \mu(r_i S(q^n) - S(p^n)) \leq \mu S(q^n) \leq \mu. \quad (45)$$

On the other hand, if $A^n(r_i) < 0$,

$$|A^n(r_i)| = \mu(S(p^n) - r_i S(q^n)) \leq \mu S(p^n) \leq \frac{\mu}{2}. \quad (46)$$

Hence, $|A^n(r_i)| \leq \mu$.

Then, it is straightforward that the main coefficient of the scheme (40) is positive if

$$\Delta t < \frac{\Delta r}{\mu}, \quad (47)$$

which corresponds to the condition that the Courant number satisfies $|C_i^n| < 1 \forall i, n$.

4.2.2 | Numerical Diffusivity

Let us expand the exact solution $w(t, r)$ at the grid point (t^n, r_i) using a Taylor series in time and space. Expanding in time gives:

$$w_i^{n+1} = w(t^n + \Delta t, r_i) = w_i^n + \Delta t \frac{\partial w}{\partial t} + \frac{\Delta t^2}{2} \frac{\partial^2 w}{\partial t^2} + O(\Delta t^3), \quad (48)$$

and expanding in space gives:

$$w_{i+\text{sign}(A^n(r_i))}^n = w(t^n, r_i + \text{sign}(A^n(r_i))\Delta r) = w_i^n + \text{sign}(A^n(r_i))\Delta r \frac{\partial w}{\partial r} + \frac{\Delta r^2}{2} \frac{\partial^2 w}{\partial r^2} + O(\Delta r^3). \quad (49)$$

Substituting these expansions into the upwind scheme, one gets

$$w_t + \frac{\Delta t}{2} w_{tt} = A^n(r_i) w_r + |A^n(r_i)| \frac{\Delta r}{2} w_{rr} + [\alpha^2 (l^n S(y^n(r_i)) - w_i^n) + f(w_i^n)] + O(\Delta t^2, \Delta r^2). \quad (50)$$

Assuming that $A^n(r_i)$ and $[\alpha^2 (l^n S(y^n(r_i)) - w_i^n) + f(w_i^n)]$ are constant at the fixed point (r_i, t^n) , we get that $w_{tt} = |A^n(r_i)|^2 w_{rr}$, hence

$$w_t = A^n(r_i) w_r + |A^n(r_i)| \frac{\Delta r}{2} (1 - |C_i^n|) w_{rr} + [\alpha^2 (l^n S(y^n(r_i)) - w_i^n) + f(w_i^n)] + O(\Delta t^2, \Delta r^2). \quad (51)$$

The upwind scheme introduces a truncation error that results in a term proportional to the second spatial derivative of w , which acts as an artificial diffusion term. Specifically, the artificial diffusivity ν_{num} can be written as:

$$\nu_{\text{num}} = \frac{1}{2} |A^n(r_i)| \Delta r (1 - |C_i^n|).$$

This artificial diffusivity acts like physical diffusion, smoothing out the solution over time. It is clear that setting Δt to give $|C_i^n| = 1$, which would avoid the artificial diffusivity, is not possible due to variations in $|A^n(r_i)|$.

4.3 | Lax-Wendroff Scheme

The Lax-Wendroff method is a well-known second-order method for solving hyperbolic partial differential equations (PDEs), particularly in fluid dynamics applications, including inviscid, compressible flow [36]. The method is effective because it combines accuracy with stability by leveraging a Taylor series expansion to achieve a second-order approximation in both time and space avoiding the artificial diffusivity.

The time derivative is approximated as follows:

$$\frac{\partial w}{\partial t} \approx \frac{w_i^{n+1} - w_i^n}{\Delta t} - \frac{\Delta t}{2} w_{tt} = \frac{w_i^{n+1} - w_i^n}{\Delta t} - \frac{\Delta t}{2} |A^n(r_i)|^2 w_{rr}. \quad (52)$$

Then, (27) is approximated as follows:

$$w_i^{n+1} = w_i^n + \frac{C_i^n}{2} (w_{i+1}^n - w_{i-1}^n) + \frac{(C_i^n)^2}{2} (w_{i+1}^n - 2w_i^n + w_{i-1}^n) + \Delta t \alpha^2 [l^n S(y^n(r_i)) - w_i^n] + \Delta t f(w_i^n). \quad (53)$$

The Lax-Wendroff scheme is conditionally stable for linear convection equation if the Courant number is less or equal to one, which corresponds, in our case, to the condition (47).

5 | Numerical Examples and Simulations

This section presents numerical examples and simulations to validate the proposed FF method and to explore the behavior of the nonlocal Fisher-KPP model. First, in Section 5.1, we compare the performance of the different numerical schemes (FTCS, upwind, and Lax-Wendroff). Section 5.2 investigates the spreading-vanishing dichotomy predicted by the theory. The impact of different kernel functions on the spreading rate is analyzed in Section 5.3. Finally, Section 5.4 examines how the initial population distribution affects the solution dynamics.

Computations have been carried out by Matlab software version R2024b for Windows 11 Home (64-bit) 11th Gen Intel(R) Core(TM) i5-11300H @ 3.10GHz 3.11 GHz.

Example 1. Let us consider the problem (1) – (7) with the following parameters:

$$h(0) = h_0 = 0.7 = -g(0), \quad \mu = 1.5, \quad \alpha^2 = 2, \quad u(0, x) = h_0^2 - x^2, \quad f(u) = 2u(1 - u), \quad J(x) = \frac{1}{\pi(1 + x^2)}. \quad (54)$$

5.1 | Comparison of the Schemes

In the preceding section, we introduced several explicit numerical schemes (FTCS, upwind, and Lax-Wendroff) to discretize the differential operator in Equation (27). For the integral approximation in all cases, we employed Simpson's quadrature rule. In this subsection, we will evaluate the performance of these schemes.

In Example 1, we set the time step size as $\Delta t = 1 \times 10^{-4}$ and investigate the spatial discretization using a set of values for M from the set $\{50, 100, 200, 400, 800, 1600\}$ for three different numerical methods. For comparison, we utilize the solution obtained from the Lax-Wendroff method with $M = 3200$ as our reference solution.

The maximum Courant number is defined as $C^* = \max_{i,n} |C_i^n| = \max_{i,n} |A^n(r_i)| \frac{\Delta t}{\Delta r}$. Table 1 reports the maximum Courant number for different numbers of spatial nodes, alongside the corresponding CPU times (in seconds) for the

TABLE 1 | Maximum Courant number $C^*(M)$ and corresponding CPU time (in seconds) for various spatial step counts M in Example 1, with $T = 50$ and a time step size of $\Delta t = 10^{-4}$.

M	50	100	200	400	800	1600
$C^*(M)$	$7.72 \cdot 10^{-4}$	$1.54 \cdot 10^{-3}$	$3.09 \cdot 10^{-3}$	$6.17 \cdot 10^{-3}$	$1.23 \cdot 10^{-2}$	$2.47 \cdot 10^{-2}$
Lax–Wendroff scheme CPU-time (s)	14.36	32.36	73.97	209.95	598.72	1622.77

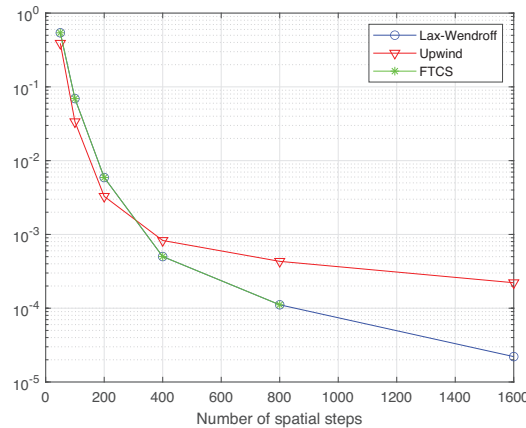


FIGURE 1 | Comparison of mean absolute errors at $t = 50$ as a function of the number of spatial discretization nodes for the FTCS, upwind, and Lax–Wendroff schemes against the reference solution. FTCS, forward-time centered-space.

Lax–Wendroff numerical scheme. Other numerical methods (upwind and FTCS) exhibit comparable performance, as the number of temporal and spatial iterations remains consistent across schemes.

To assess the accuracy of the various methods, we compare the computed solutions at time $t = T = 50$ employing cubic spline interpolation. The resulting mean absolute errors, illustrated in Figure 1, are calculated based on the number of spatial discretization nodes. Notably, we observe oscillatory behavior in the numerical solutions for $M < 300$. This phenomenon can be attributed to the inverse FF transformation employed to derive the solutions in the original variable space. This oscillatory effect has been similarly documented in previous research [28], where it was demonstrated that the FF method loses accuracy over extended time horizons if the spatial stepsize is not diminishing. Consequently, it is advisable to select a sufficiently large M when dealing with large values of T to mitigate this limitation. However, for $M > 800$, the FTCS scheme becomes unstable, resulting in the generation of NaN (not a number) values in the computed solutions.

Analogously, taking into account previous comments about spatial discretization, we set $M = 300$ and consider $N \in \{10^3, 2 \cdot 10^3, 4 \cdot 10^3, 8 \cdot 10^3, 16 \cdot 10^3\}$ for three considered methods. In Figure 2, mean absolute errors as a function of the number of temporal discretization steps computed at $t = T$ using cubic spline interpolation are presented.

Note that the maximum Courant number $C^*(N) < 1$ for $N > 2 \cdot 10^3$. However, for $N = 2 \cdot 10^3$, $C^* = 1.1574$, which exceeds the stability threshold. This can lead to numerical instabilities and a loss of accuracy in the solution. This behavior explains the non-monotonic trend observed for smaller N in the mean absolute errors shown in Figure 2).

In both plots, the Lax–Wendroff scheme consistently demonstrates superior performance compared to the other methods. In contrast, the upwind scheme exhibits the slowest convergence, likely attributable to numerical diffusion. In further examples, we employ the Lax–Wendroff scheme (53).

5.2 | Spreading-Vanishing Dichotomy Study

Now, let us examine the theoretical results regarding the spreading–vanishing dichotomy proposed in [23]. According to this theory, vanishing occurs if $f'(0) < \alpha^2$, $h_0 < \ell^*/2$, and $\mu \leq \mu^*$, where ℓ^* and μ^* are some positive constants to be determined.

In the case of the parameters given by (54), where $f'(0) = \alpha^2 = 2$, spreading always occurs, independent of the choice of h_0 and μ . However, if we consider a family of functions $f_\gamma(u) = \gamma u(1 - u)$ as the growth term, we expect to observe

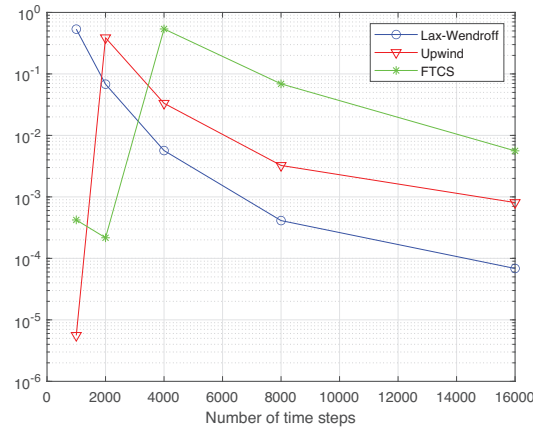


FIGURE 2 | Comparison of mean absolute errors at $t = 50$ as a function of the number of time levels for the FTCS, upwind, and Lax-Wendroff schemes against the reference solution. FTCS, forward-time centered-space.

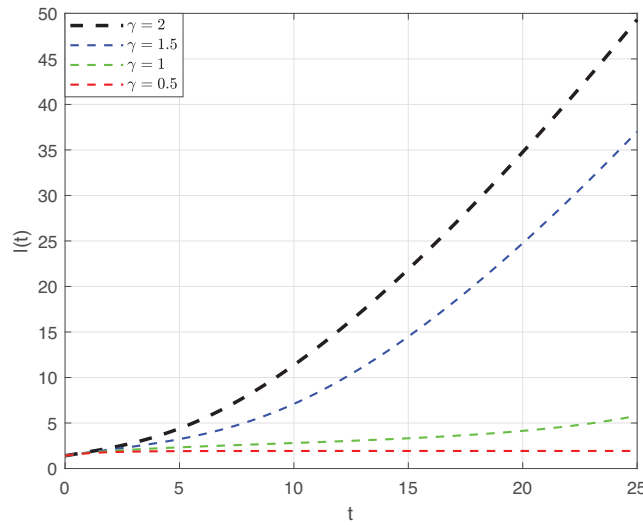


FIGURE 3 | Evolution of $l(t)$ for various growth term $f_\gamma(u) = \gamma u(1 - u)$.

both spreading and vanishing scenarios. For this analysis, we extend the time horizon to $T = 25$, while the rest of the parameters remain the same as taken in (54). The evolution of $l(t)$ for $t \in [0, 25]$ for various γ is plotted in Figure 3. For $\gamma = 1$, the length of the domain $l(t) = h(t) - g(t)$ is increasing but tends to some constant $C < \infty$.

Now, we set $f(u) = u(1 - u)$ as a boundary case and vary h_0 to observe spreading–vanishing dichotomy (see Figure 4). If $h_0 < 0.7$, the vanishing observed, however, for $h_0 > 0.7$, the spreading occurs. Note that here we do not pretend that $h_0 = 0.7$ is a threshold value $\ell^*/2$, but it can be considered an initial guess for the approximation.

We now set $f(u) = u(1 - u)$ as a boundary case and vary h_0 to examine the spreading–vanishing dichotomy (see Figure 4). When $h_0 < 0.7$, vanishing is observed, whereas for $h_0 > 0.7$, spreading occurs. It is important to note that we do not claim $h_0 = 0.7$ to be the exact threshold value $\ell^*/2$; rather, it can be considered an initial estimate for this threshold.

Finally, we consider $f(u) = u(1 - u)$ with $h_0 = 0.5$ (resulting in vanishing, as shown in Figure 4) and vary μ to examine the spreading–vanishing dichotomy (see Figure 5). When $\mu \geq 5$, spreading occurs. This indicates that there exists a critical value μ^* such that if $\mu > \mu^*$, spreading will happen.

5.3 | Impact of Kernel Function

Let us analyze and compare several kernel functions listed in Table 2 (see Figure 6):

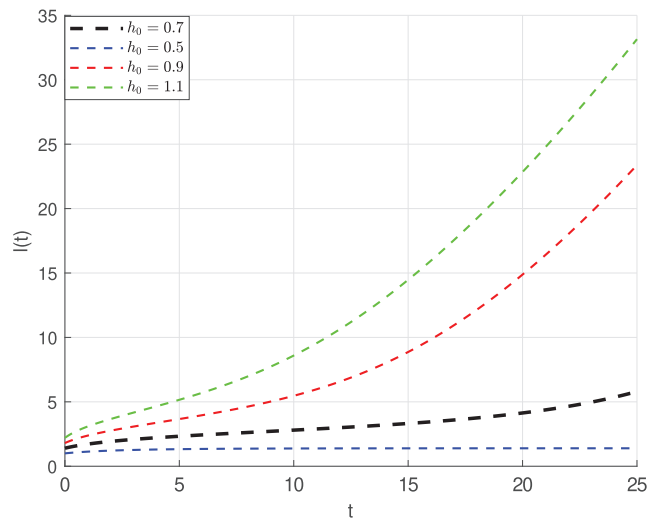


FIGURE 4 | Evolution of $l(t)$ for the growth term $f(u) = u(1 - u)$ and various h_0 .

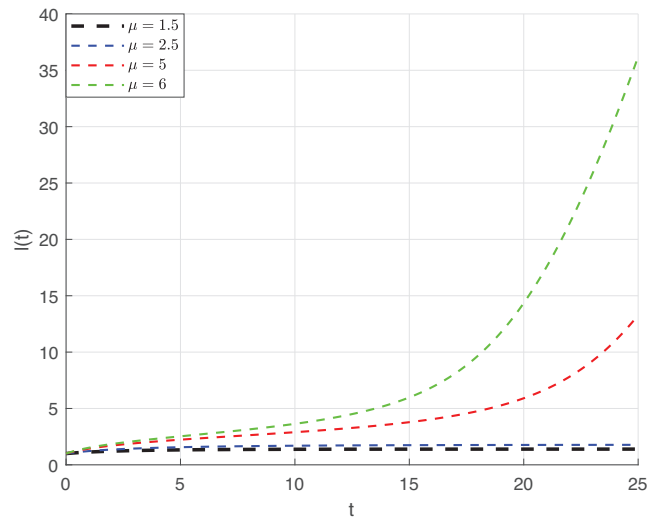


FIGURE 5 | Evolution of $l(t)$ for the growth term $f(u) = u(1 - u)$, $h_0 = 0.5$ and various μ .

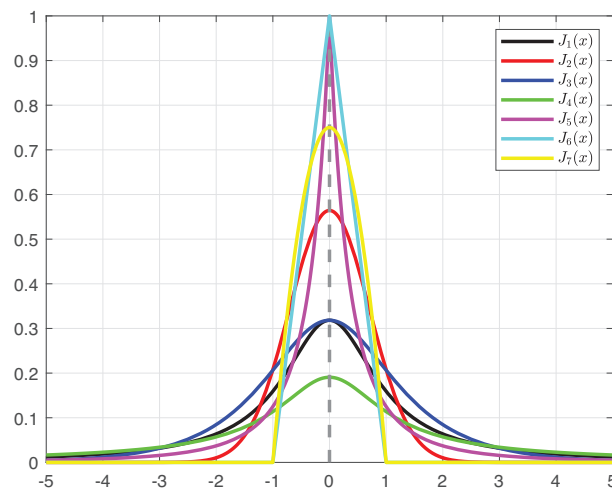


FIGURE 6 | Kernel functions given in Table 2.

TABLE 2 | Kernel functions and corresponding integrals.

$J(x)$	$K[x] = \int_{-\infty}^x J(s) ds$
$J_1(x) = \frac{1}{\pi(1+x^2)}$	$K_1[x] = \frac{\arctan x}{\pi} + \frac{1}{2}$
$J_2(x) = \frac{e^{-x^2}}{\sqrt{\pi}}$	$K_2[x] = \frac{\text{erf}(x)+1}{2}$
$J_3(x) = \frac{\text{sech } x}{\pi}$	$K_3[x] = \frac{2}{\pi} \arctan(e^x)$
$J_4(x) = \frac{\Gamma(\frac{3}{4})}{\sqrt{\pi}\Gamma(\frac{1}{4})(1+x^2)^{3/4}}$	$K_4[x] = \frac{1}{2} + \frac{\Gamma(\frac{3}{4})}{\sqrt{\pi}\Gamma(\frac{1}{4})} x(1+x^2)^{1/4} {}_2F_1\left(\frac{3}{4}, 1; \frac{3}{2}; -x^2\right)$
$J_5(x) = \frac{1}{(1+ x)^3}$	$K_5[x] = \begin{cases} \frac{1}{2(x-1)^2}, & \text{if } x < 0 \\ 1 - \frac{1}{2(x+1)^2}, & \text{if } x \geq 0 \end{cases}$
$J_6(x) = \begin{cases} 1 - x , & \text{if } x \in [-1, 1] \\ 0, & \text{otherwise} \end{cases}$	$K_6[x] = \begin{cases} 0 & \text{if } x \leq -1 \\ \frac{(x+1)^2}{2} & \text{if } x \in (-1, 0) \\ \frac{-x^2+2x+1}{2} & \text{if } x \in [0, 1) \\ 1 & \text{if } x \geq 1 \end{cases}$
$J_7(x) = \begin{cases} \frac{3}{4}(1-x^2), & \text{if } x \in [-1, 1] \\ 0, & \text{otherwise} \end{cases}$	$K_7[x] = \begin{cases} 0 & \text{if } x \leq -1 \\ \frac{-x^3+3x+2}{4} & \text{if } x \in (-1, 1) \\ 1 & \text{if } x \geq 1 \end{cases}$

1. Kernel $J_1(x)$ is the Cauchy distribution, characterized by its heavy tails and peak at $x = 0$. This function decays as $|x|^{-2}$ for large $|x|$.
2. $J_2(x)$ is the Gaussian kernel, characterized by rapid exponential decay satisfying so-called thin-tail condition. The cumulative function uses the error function $\text{erf}(x)$.
3. $J_3(x)$ is based on the hyperbolic secant function $\text{sech}(x)$. It has exponential decay similar to the Gaussian.
4. $J_4(x)$ has a decay behavior proportional to $|x|^{-3/2}$, where the decay rate is slower than the Gaussian kernel. The cumulative function $K_4[x]$ involves the hypergeometric function ${}_2F_1(a, b; c; d)$, capturing the non-elementary integral behavior.
5. $J_5(x)$ is a kernel with polynomial decay, $J_5(x) \sim |x|^{-3}$. It is heavy-tailed but satisfies the first-moment condition (10).
6. $J_6(x)$ is a triangular kernel compactly supported within $[-1, 1]$. It is piece-wise-linear, peaking at $x = 0$, and decays linearly to 0 at $x = \pm 1$.
7. $J_7(x)$ is a parabolic kernel compactly supported within $[-1, 1]$.

The evolution of the habitat, $h(t)$, over time, is shown for each kernel in Figure 7. The results are consistent with previous theoretical findings for nonlocal diffusion problems discussed in [25, 26]. Specifically, in the case of spreading, it has a finite speed if and only if condition (10) is satisfied; otherwise, spreading becomes accelerated. While kernels with compact support ($J_6(x)$ and $J_7(x)$) exhibit asymptotically linear spreading behavior, they are not fat-tailed (equal to zero if $|x| > 1$) and therefore, they are less relevant for further exploration of accelerated propagation dynamics.

Among the kernels examined, $J_1(x)$ and $J_4(x)$ fail to satisfy the first-moment condition (10) (see the third column of Table 3). Specifically, for $J_1(x) \sim |x|^{-2}$ as $|x| \rightarrow \infty$, we have:

$$\lambda_1 = \lim_{x \rightarrow \infty} J_1(x)x^2 = \lim_{x \rightarrow \infty} \frac{x^2}{\pi(1+x^2)} = \frac{1}{\pi}. \quad (55)$$

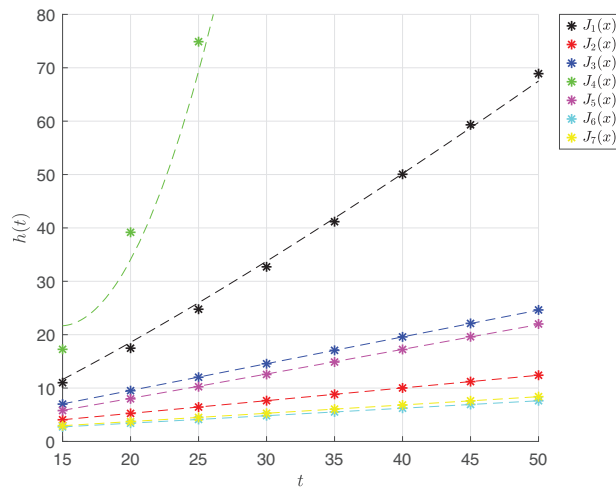


FIGURE 7 | Free boundary $h(t)$ over time for various kernel functions and parameters given in (54). Dashed lines represent the corresponding regression curves.

TABLE 3 | Kernel functions and characteristics.

$J(x)$	$\int_0^\infty xJ(x)dx$	Thin/heavy tail	Spreading rate
$J_1(x) = \frac{1}{\pi(1+x^2)}$	∞	Heavy	$\lim_{t \rightarrow \infty} \frac{h(t)}{t \ln t} = \frac{\mu}{\pi}$
$J_2(x) = \frac{e^{-x^2}}{\sqrt{\pi}}$	$\frac{1}{2\sqrt{\pi}}$	Thin	$\lim_{t \rightarrow \infty} \frac{h(t)}{t} = c_0 = 0.2381$
$J_3(x) = \frac{\text{sech } x}{\pi}$	$\frac{2G}{\pi}$	Thin	$\lim_{t \rightarrow \infty} \frac{h(t)}{t} = c_0 = 0.5019$
$J_4(x) = \frac{\Gamma(\frac{3}{4})}{\sqrt{\pi}\Gamma(\frac{1}{4})(1+x^2)^{3/4}}$	∞	Heavy	$\lim_{t \rightarrow \infty} \frac{h(t)}{t^2} = \frac{2\sqrt{2}\Gamma(\frac{3}{4})}{\sqrt{\pi}\Gamma(\frac{1}{4})}\mu$
$J_5(x) = \frac{1}{(1+ x)^3}$	$\frac{1}{2}$	Heavy	$\lim_{t \rightarrow \infty} \frac{h(t)}{t} = c_0 = 0.4759$

Note: Here, G is Catalan constant, $G \approx 0.91597$.

Therefore, according to (14), the spreading rate is:

$$\lim_{t \rightarrow \infty} \frac{h(t)}{t \ln t} = \frac{\mu}{\pi}. \quad (56)$$

Numerically, by fitting the regression equation $LR(t \ln t) = c_0 t \ln t + c_1$, we obtain $c_0 = 0.4247$, which closely approximates the theoretical value $c_0^* = \frac{\mu}{\pi} = 0.4775$. This agreement validates the accuracy of our numerical algorithm in capturing the theoretical accelerated spreading rate. The coefficient of determination is $R^2 = 0.9974$, such a high degree of fit confirms that the observed spreading behavior closely follows the expected asymptotic form.

Similarly, for $J_4(x) \sim |x|^{-3/2}$ as $|x| \rightarrow \infty$, we compute:

$$\lambda_4 = \lim_{x \rightarrow \infty} J_4(x)x^{3/2} = \lim_{x \rightarrow \infty} \frac{\Gamma(\frac{3}{4})x^{3/2}}{\sqrt{\pi}\Gamma(\frac{1}{4})(1+x^2)^{3/4}} = \frac{\Gamma(\frac{3}{4})}{\sqrt{\pi}\Gamma(\frac{1}{4})} \approx 0.1907. \quad (57)$$

Thus, from (13), the spreading rate is:

$$\lim_{t \rightarrow \infty} \frac{h(t)}{t^2} = \frac{\sqrt{2}}{1/2} \mu \lambda_4 = \frac{2\sqrt{2}\Gamma(\frac{3}{4})}{\sqrt{\pi}\Gamma(\frac{1}{4})} \mu. \quad (58)$$

TABLE 4 | Initial population density function and corresponding characteristics.

$u_0(x)$	$P(0) = \int_{-h_0}^{h_0} u_0(x) dx$	$\max_{x \in [h_0, h_0]} u_0(x)$	Observations
$u_0(x) = h_0^2 - x^2$	0.4573	0.4900	Symmetric unimodal
$u_0^1(x) = \cos\left(\pi \frac{x}{h_0}\right) + \cos\left(3\pi \frac{x}{h_0}\right) + 2$	2.8000	3.9950	Symmetric multimodal
$u_0^2(x) = \left(\frac{x}{h_0}\right)^3 - 1.2\left(\frac{x}{h_0}\right)^2 - \left(\frac{x}{h_0}\right) + 1.2$	1.1200	1.3648	Asymmetric unimodal
$u_0^3(x) = -\left(\frac{x}{h_0}\right)^4 + 0.4\left(\frac{x}{h_0}\right)^3 + 0.71\left(\frac{x}{h_0}\right)^2 - 0.4\left(\frac{x}{h_0}\right) + 0.29$	0.4573	0.5697	Asymmetric multimodal

Numerically, by fitting the parabolic regression equation $PR(t) = c_0 t^2 + c_1 t + c_2$ to the data for the range of values $T = \{30, 35, 40, 45\}$, we obtain $c_0 = 0.8535$ with a coefficient of determination $R^2 = 0.9996$. This high R^2 value indicates a good fit between the regression model and the numerical data, demonstrating the strong reliability of the fit. The obtained numerical value c_0 approximates the theoretical value $c_0^* = 0.8091$ with high accuracy. Larger values of T were specifically chosen to better capture the parabolic asymptotic behavior, as smaller values of T do not accurately reflect the long-term quadratic growth. This approach ensures a more precise estimation of the asymptotic coefficients.

In contrast, kernels $J_2(x)$ and $J_3(x)$ satisfy the first-moment condition (10), meaning their asymptotic behavior is linear. To calculate the spreading rate, we performed a series of simulations with $T = 5, 10, \dots, 50$, and fitted a linear regression of the form $LR(t) = c_0 t + c_1$ with $R^2 = 1$.

Finally, the kernel $J_5(x)$ satisfies the first-moment condition (10), but it does not satisfy the thin-tail condition (12). Specifically, since $J_5(x) \sim |x|^{-3}$ as $|x| \rightarrow \infty$, it falls into a class of kernels with heavy tails, where the decay rate of the kernel is slower than what is required by the thin-tail condition. According to the results in [46], this behavior implies that the difference $c_0 t - h(t)$ asymptotically behaves as $\ln t$. Consequently, the regression equation for the asymptotic growth takes the form $LLR(t) = c_0 t + c_1 \ln t$. Based on numerical fitting, we obtain $c_0 = 0.4759$. The coefficient of determination is $R^2 = 0.99973$.

In conclusion, our numerical simulations confirm that spreading occurs at finite speeds when the kernel satisfies the first-moment condition (10), while accelerated spreading arises when this condition is violated. For thin-tailed kernels, such as $J_2(x)$ and $J_3(x)$, spreading remains linear, consistent with theoretical predictions. In contrast, fat-tailed kernels like $J_1(x)$ and $J_4(x)$ exhibit logarithmic or quadratic spreading rates, reflecting the kernel's influence on the population's dispersal patterns. Figure 7 visually highlights these distinctions.

5.4 | Impact of the Shape of Initial Population

Next, let us examine the impact of the initial conditions.

Example 2. Let us consider the problem (1)–(7) with the following parameters:

$$h(0) = h_0 = 0.7 = -g(0), \quad \mu = 1.5, \quad \alpha^2 = 2, \quad f(u) = 2u(1 - u), \quad J(x) = \frac{1}{\pi(1 + x^2)}, \quad T = 1, \quad (59)$$

and vary the initial population function $u_0(x)$.

First, let us consider $u_0(x) = h_0^2 - x^2$. Integrating this function over interval $[-h_0, h_0]$ we obtain the initial population $P(t = 0) = 0.45$. Moreover, $\max_{x \in [h_0, h_0]} u_0(x) = h_0^2$, which is less than the carrying capacity K that is equal to 1. Initial and final (at $T = 1$) solutions are presented in Figure 7, black and blue lines, respectively.

Now, let us consider the initial density functions given in Table 4.

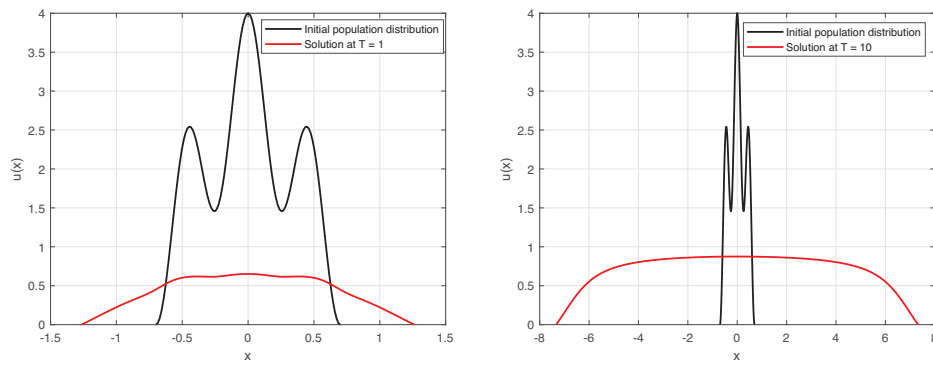


FIGURE 8 | Initial and final density distribution at $T = 1, 10$ for $u_0^1(x) = \cos\left(\pi \frac{x}{h_0}\right) + \cos\left(3\pi \frac{x}{h_0}\right) + 2$.

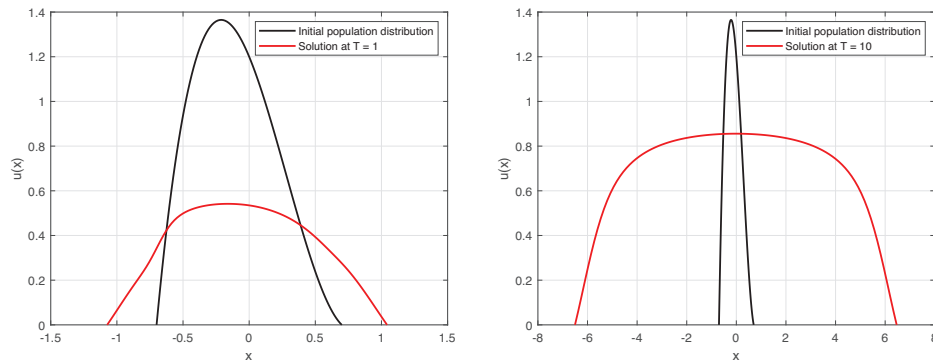


FIGURE 9 | Initial and final density distribution at $T = 1, 10$ for $u_0^2(x) = \left(\frac{x}{h_0}\right)^3 - 1.2\left(\frac{x}{h_0}\right)^2 - \left(\frac{x}{h_0}\right) + 1.2$.

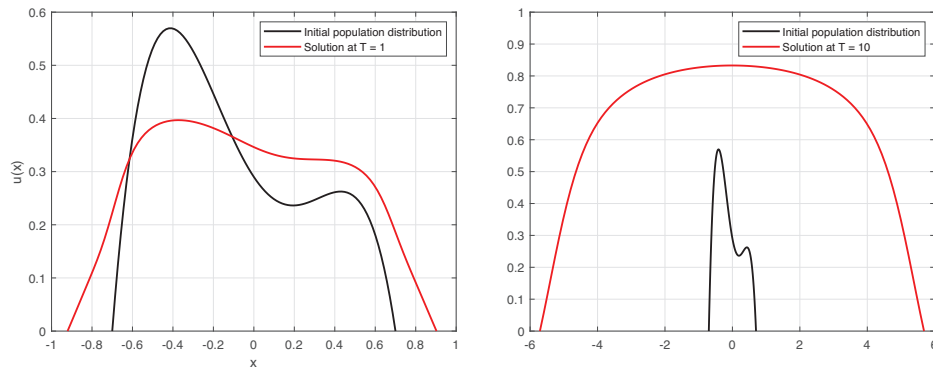


FIGURE 10 | Initial and final density distribution at $T = 1, 10$ for $u_0^3(x) = -\left(\frac{x}{h_0}\right)^4 + 0.4\left(\frac{x}{h_0}\right)^3 + 0.71\left(\frac{x}{h_0}\right)^2 - 0.4\left(\frac{x}{h_0}\right) + 0.29$.

The initial population distributions from Table 4, denoted by $u_0^1(x)$, $u_0^2(x)$ and $u_0^3(x)$, are illustrated in Figures 8–10, respectively. The corresponding numerical solutions at times $T = 1$ and $T = 10$ are also shown. Regardless of the initial distribution, the numerical solution consistently converges to a symmetric unimodal pattern.

For the given parameters in Equation (59), the carrying capacity is 1. Even when the initial population exceeds this limit (see column $\max_{x \in [h_0, h_0]} u_0(x)$ in Table 4), the solution approaches the theoretical boundaries. While symmetry and unimodality are observed in all cases, the convergence to this pattern is slower for the more complex, asymmetric, multimodal initial density $u_0^3(x)$.

6 | Conclusion

In this study, we developed and analyzed a numerical method for solving 1D nonlocal diffusion models with free boundaries, focusing on the Fisher-KPP framework. This research builds upon and extends numerically the foundational theoretical studies [23, 25, 26], offering a robust numerical perspective to explore and validate the qualitative properties of the model.

A key novelty of our approach lies in the successful adaptation and application of a two-stage FF transformation. This technique effectively addressed the challenges posed by moving boundaries, reformulating the original ordinary integro-differential equation (OIDE) with a free boundary into a PIDE on a fixed spatial domain. This transformation enabled the application of established numerical techniques, including several explicit finite difference methods (FTCS, upwind, and Lax–Wendroff) and quadrature rules for integral approximations. We established stability conditions for these schemes, notably for the upwind method, and demonstrated the superior accuracy and stability balance of the Lax–Wendroff scheme for this class of transformed problems.

Our numerical simulations confirm the accuracy and efficiency of the proposed method in capturing the dynamics of population spreading and boundary movement. The method demonstrated flexibility by successfully handling diverse initial conditions and various kernel functions, including those leading to accelerated spreading. Through these simulations, we numerically validated key theoretical results, such as the spreading–vanishing dichotomy, where the population either expands indefinitely or contracts to extinction depending on the growth parameters and initial conditions. Furthermore, we investigated the rate of accelerated spreading for fat-tailed kernels, highlighting how these rates deviate from classical linear spreading and providing deeper insights into the influence of kernel properties on propagation dynamics. These findings reinforce the method’s robustness and its utility in studying complex nonlocal diffusion models. The computational efficiency demonstrated is an important prerequisite before extending this methodology to more complex scenarios.

Overall, the FF transformation coupled with appropriate finite difference schemes provides a reliable and efficient framework for studying population models with nonlocal diffusion and evolving boundaries. This work highlights the originality of extending FF techniques to effectively tackle the combined complexities of nonlocality and free boundaries. While presented here in one dimension, this study serves as a crucial first step. Future work will focus on extending this approach to higher-dimensional problems, potentially leveraging symmetries (such as radial symmetry in 2D, which can reduce to 1D nonlocal problems as seen in recent literature [49]) and investigating models with random parameters or more complex ecological interactions.

Author Contributions

M.C. Casabán: conceptualization, methodology. **Rafael Company:** conceptualization, methodology, supervision, writing – reviewing and editing. **Vera Egorova:** writing – original draft preparation, investigation, software, visualization. **Mohamed El Fakharany:** methodology, validation, writing – reviewing and editing. **Lucas Jódar:** conceptualization, supervision.

Conflicts of Interest

The authors declare no potential conflicts of interest.

Data Availability Statement

Data sharing not applicable to this article as no datasets were generated or analyzed during the current study. The code used in this research is openly available and can be accessed at the following repository: <https://github.com/RaVeX-Numerics/NonlocalDiffusionFF>

References

1. R. A. Fisher, “The Wave of Advance of Advantageous Genes,” *Annals of Eugenics* 7 (1937): 355–369, <https://doi.org/10.1111/j.1469-1809.1937.tb02153.x>.
2. A. Kolmogorov, N. Petrovsky, and S. Piscounov, “Étude de l’équations de la diffusion Avec Croissance de la Quantité de Matière et Son Application a un problème Biologique,” *Bulletin of Moscow University* 1 (1937): 1–25.
3. D. G. Aronson and H. F. Weinberger, “Multidimensional Nonlinear Diffusion Arising in Population Genetics,” *Advances in Mathematics* 30 (1978): 33–76, [https://doi.org/10.1016/0001-8708\(78\)90130-5](https://doi.org/10.1016/0001-8708(78)90130-5).
4. M. Kot, *Elements of Mathematical Ecology* (Cambridge University Press, 2001).
5. L. Edelstein-Keshet, *Mathematical Models in Biology* (Society for Industrial and Applied Mathematics, 2005).

6. H. Malchow, *Spatiotemporal Patterns in Ecology and Epidemiology* (Chapman and Hall, 2007).
7. M. Bengfort, H. Malchow, and F. M. Hilker, "The Fokker-Planck Law of Diffusion and Pattern Formation in Heterogeneous Environments," *Journal of Mathematical Biology* 73 (2016): 683–704, <https://doi.org/10.1007/s00285-016-0966-8>.
8. A. Okubo and S. A. Levin, *Diffusion and Ecological Problems: Modern Perspectives*, vol. 14 (Springer, 2001).
9. Z. Li and B. Dai, "Long-Time Behavior of a Nonlocal Dispersal Logistic Model With Seasonal Succession," *Mathematics in Applied Sciences and Engineering* 3 (2022): 249–268, <https://doi.org/10.5206/mase/15415>.
10. A. Ducrot and Z. Jin, "Spreading Properties for Non-Autonomous Fisher-KPP Equations With Non-Local Diffusion," *Journal of Nonlinear Science* 33 (2023): 100, <https://doi.org/10.1007/s00332-023-09954-6>.
11. H. Berestycki, J. Coville, and H. H. Vo, "Persistence Criteria for Populations With Non-Local Dispersion," *Journal of Mathematical Biology* 72 (2016): 1693–1745, <https://doi.org/10.1007/s00285-015-0911-2>.
12. F. Lutscher, E. Pachepsky, and M. A. Lewis, "The Effect of Dispersal Patterns on Stream Populations," *SIAM Review* 47 (2005): 749–772, <https://doi.org/10.1137/050636152>.
13. C. Feng, M. A. Lewis, C. Wang, and H. Wang, "A Fisher-KPP Model With a Nonlocal Weighted Free Boundary: Analysis of How Habitat Boundaries Expand, Balance or Shrink," *Bulletin of Mathematical Biology* 84 (2022): 34, <https://doi.org/10.1007/s11538-022-00995-8>.
14. Y. Du, "Propagation and Reaction-Diffusion Models With Free Boundaries," *Bulletin of Mathematical Sciences* 12 (2022): 2230001, <https://doi.org/10.1142/S1664360722300018>.
15. R. Yi, Y. Cohen, H. Seybold, et al., "A Free-Boundary Model of Diffusive Valley Growth: Theory and Observation," *Proceedings of the Royal Society A: Mathematical, Physical and Engineering Sciences* 473 (2017): 20170159, <https://doi.org/10.1098/rspa.2017.0159>.
16. I. Ahn, S. Baek, and Z. Lin, "The Spreading Fronts of an Infective Environment in a Man-Environment-man Epidemic Model," *Applied Mathematical Modelling* 40 (2016): 7082–7101, <https://doi.org/10.1016/j.apm.2016.02.038>.
17. Y. Hu, X. Hao, X. Song, and Y. Du, "A Free Boundary Problem for Spreading Under Shifting Climate," *Journal of Differential Equations* 269 (2020): 5931–5958, <https://doi.org/10.1016/j.jde.2020.04.024>.
18. S. L. Mitchell and S. B. G. O'Brien, "Asymptotic and Numerical Solutions of a Free Boundary Problem for the Sorption of a Finite Amount of Solvent into a Glassy Polymer," *SIAM Journal on Applied Mathematics* 74 (2014): 697–723, <https://doi.org/10.1137/120899200>.
19. B. F. Nielsen, O. Skavhaug, and A. Tvelto, "Penalty and Front-Fixing Methods for the Numerical Solution of American Option Problems," *Journal of Computational Finance* 5 (2002): 69–97.
20. R. Company, V. N. Egorova, and L. Jódar, "An ETD Method for Multi-asset American Option Pricing Under Jump-Diffusion model," *Mathematical Methods in the Applied Sciences* 46 (2023): 10332–10347, <https://doi.org/10.1002/mma.9125>.
21. K. M. Moroney, L. Kotamarchy, I. Muthancheri, R. Ramachandran, and M. Vynnycky, "A Moving-Boundary Model of Dissolution From Binary Drug-Excipient Granules Incorporating Microstructure," *International Journal of Pharmaceutics* 599 (2021): 120219, <https://doi.org/10.1016/j.ijpharm.2021.120219>.
22. M. Vynnycky, "On Boundary Immobilization for One-Dimensional Stefan-Type Problems With a Moving Boundary Having Initially Parabolic-Logarithmic Behaviour," *Applied Mathematics and Computation* 444 (2023): 127803, <https://doi.org/10.1016/j.amc.2022.127803>.
23. J. F. Cao, Y. Du, F. Li, and W. T. Li, "The Dynamics of a Fisher-KPP Nonlocal Diffusion Model With Free Boundaries," *Journal of Functional Analysis* 277 (2019): 2772–2814, <https://doi.org/10.1016/j.jfa.2019.02.013>.
24. Y. Du and Z. Lin, "Spreading-Vanishing Dichotomy in the Diffusive Logistic Model With a Free Boundary," *SIAM Journal on Mathematical Analysis* 42 (2010): 377–405, <https://doi.org/10.1137/090771089>.
25. Y. Du, F. Li, and M. Zhou, "Semi-Wave and Spreading Speed of the Nonlocal Fisher-KPP Equation With Free Boundaries," *Journal des Mathématiques Pures et Appliquées* 154 (2021): 30–66, <https://doi.org/10.1016/j.matpur.2021.08.008>.
26. Y. Du and W. Ni, "Exact Rate of Accelerated Propagation in the Fisher-KPP Equation With Nonlocal Diffusion and Free Boundaries," *Mathematische Annalen* 389 (2024): 2931–2958, <https://doi.org/10.1007/s00208-023-02706-7>.
27. H. G. Landau, "Heat Conduction in a Melting Solid," *Quarterly Applied Mathematics* 8 (1950): 81–95.
28. M. C. Casabán, R. Company, V. N. Egorova, and L. Jódar, "Qualitative Numerical Analysis of a Free-Boundary Diffusive Logistic Model," *Mathematics* 11 (2023): 1296, <https://doi.org/10.3390/math11061296>.
29. L. Jain, J. Joshi, and Rajeev, "A Numerical Approach to a Two-Phase Free Boundary Problem With MPC Material in a Finite Domain," *International Journal of Numerical Methods for Heat & Fluid Flow* (2024), <https://doi.org/10.1108/HFF-09-2024-0702>.
30. S. Nepal, M. Ögren, Y. Wondmagegne, and A. Muntean, "Random Walks and Moving Boundaries: Estimating the Penetration of Diffusants into Dense Rubbers," *Probabilistic Engineering Mechanics* 74 (2023): 103546, <https://doi.org/10.1016/j.probengmech.2023.103546>.
31. T. Aiki, K. Kumazaki, and A. Muntean, "A Free Boundary Problem Describing Migration into Rubbers—Quest for the Large Time Behavior," *ZAMM - Journal of Applied Mathematics and Mechanics / Zeitschrift für Angewandte Mathematik und Mechanik* 102 (2022): e202100134, <https://doi.org/10.1002/zamm.202100134>.

32. R. Fazio, A. Insana, and A. Jannelli, "A Front-Fixing Implicit Finite Difference Method for the American Put Options Model," *Mathematical and Computational Applications* 26 (2021): 30, <https://doi.org/10.3390/mca26020030>.
33. L. Wu and Y. K. Kwok, "A Front-Fixing Method for the Valuation Of American Option," *The Journal of Financial Engineering* 6 (1997): 83–97.
34. M. Vynnycky, "An Asymptotic Model for the Primary Drying Stage of Vial Lyophilization," *Journal of Engineering Mathematics* 96 (2016): 175–200, <https://doi.org/10.1007/s10665-015-9789-7>.
35. G. D. Smith, *Numerical Solution of Partial Differential Equations: Finite Difference Methods*, 3rd ed. (Clarendon Press, 1985).
36. C. A. J. Fletcher, *Computational Techniques for Fluid Dynamics 1*, 2nd ed. (Springer, 1998).
37. J. Crank, *Free and Moving Boundary Problems* (Oxford University Press, 1984).
38. S. Osher and J. A. Sethian, "Fronts Propagating With Curvature-Dependent Speed: Algorithms Based on Hamilton–Jacobi Formulations," *Journal of Computational Physics* 79 (1988): 12–49, [https://doi.org/10.1016/0021-9991\(88\)90002-2](https://doi.org/10.1016/0021-9991(88)90002-2).
39. J. A. Sethian, "Evolution, Implementation, and Application of Level Set and Fast Marching Methods for Advancing Fronts," *Journal of Computational Physics* 169 (2001): 503–555, <https://doi.org/10.1006/jcph.2000.6657>.
40. D. Gillespie, "Master Equations for Random Walks With Arbitrary Pausing Time Distributions," *Physics Letters A* 64 (1977): 22–24, [https://doi.org/10.1016/0375-9601\(77\)90513-8](https://doi.org/10.1016/0375-9601(77)90513-8).
41. K. Jiang, L. Ju, J. Li, and X. Li, "Unconditionally Stable Exponential Time Differencing Schemes for the Mass-Conserving Allen–Cahn Equation With Nonlocal and Local Effects," *Numerical Methods for Partial Differential Equations* 38 (2022): 1636–1657, <https://doi.org/10.1002/num.22827>.
42. M. Klar, C. Vollmann, and V. Schulz, "Nlfem: A Flexible 2d FEM Python Code for Nonlocal Convection-Diffusion and Mechanics," *Journal of Peridynamics and Nonlocal Modeling* 6 (2024): 87–117, <https://doi.org/10.1007/s42102-023-00108-6>.
43. Y. Fan, H. You, and Y. Yu, "OBMeshfree: An Optimization-Based Meshfree Solver for Nonlocal Diffusion and Peridynamics Models," *Journal of Peridynamics and Nonlocal Modeling* 6 (2024): 4–32, <https://doi.org/10.1007/s42102-023-00099-4>.
44. R. Courant, E. Isaacson, and M. Rees, "On the Solution of Nonlinear Hyperbolic Differential Equations by Finite Differences," *Communications on Pure and Applied Mathematics* 5 (1952): 243–255, <https://doi.org/10.1002/cpa.3160050303>.
45. P. Lax and B. Wendroff, "Systems of Conservation Laws," *Communications on Pure and Applied Mathematics* 13 (1960): 217–237, <https://doi.org/10.1002/cpa.3160130205>.
46. Y. Du and W. Ni, "Rate of Propagation for the Fisher-KPP Equation With Nonlocal Diffusion and Free Boundaries," *Journal of the European Mathematical Society* 27 (2023): 1267–1319, <https://doi.org/10.4171/jems/1392>.
47. Y. Du and Z. Guo, "Spreading-Vanishing Dichotomy in a Diffusive Logistic Model With a Free Boundary, II," *Journal of Differential Equations* 250 (2011): 4336–4366, <https://doi.org/10.1016/j.jde.2011.02.011>.
48. P. J. Davis and P. Rabinowitz, *Methods of Numerical Integration*, 2nd ed. (Academic Press Inc., 1984).
49. Y. Du and W. Ni, "The High-Dimensional Fisher-KPP Nonlocal Diffusion Equation With Free Boundary and Radial Symmetry, Part 2: Sharp Estimates," *Journal of Functional Analysis* 287 (2024): 110649, <https://doi.org/10.1016/j.jfa.2024.110649>.